

# Self-assembled artificial cilia

Mojca Vilfan<sup>a,1</sup>, Anton Potočnik<sup>a</sup>, Blaž Kavčič<sup>b</sup>, Natan Osterman<sup>a,c</sup>, Igor Poberaj<sup>c</sup>, Andrej Vilfan<sup>a</sup>, and Dušan Babič<sup>c</sup>

<sup>a</sup>J. Stefan Institute, Jamova 39, 1000 Ljubljana, Slovenia; <sup>b</sup>LPKF Laser & Elektronika, d.o.o., Polica 33, 4202 Naklo, Slovenia; and <sup>c</sup>Faculty of Mathematics and Physics, University of Ljubljana, Jadranska 19, 1000 Ljubljana, Slovenia

Edited by Tom C. Lubensky, University of Pennsylvania, Philadelphia, PA, and approved October 13, 2009 (received for review June 17, 2009)

**Due to their small dimensions, microfluidic devices operate in the low Reynolds number regime. In this case, the hydrodynamics is governed by the viscosity rather than inertia and special elements have to be introduced into the system for mixing and pumping of fluids. Here we report on the realization of an effective pumping device that mimics a ciliated surface and imitates its motion to generate fluid flow. The artificial biomimetic cilia are constructed as long chains of spherical superparamagnetic particles, which self-assemble in an external magnetic field. Magnetic field is also used to actuate the cilia in a simple nonreciprocal manner, resulting in a fluid flow. We prove the concept by measuring the velocity of a cilia-pumped fluid as a function of height above the ciliated surface and investigate the influence of the beating asymmetry on the pumping performance. A numerical simulation was carried out that successfully reproduced the experimentally obtained data.**

biomimetics | microfluidics | colloids | low Reynolds number | hydrodynamics

Efficient pumping and mixing of fluids in microscopic channels is paramount in microfluidic applications (1, 2). Small characteristic dimensions of such devices result in very low Reynolds numbers and one encounters hydrodynamics that is conceptually different from the turbulent macroscopic world. As stated by Purcell's "scallop theorem," nonreciprocal motion is required for generation of fluid flow or directed swimming (3). This is clearly manifested in biological systems, for instance in bending waves of sperm tails or in corkscrew motion of bacterial flagella. Another example are cilia, flexible protrusions on the surface of many eukaryotic cells with a typical length of several micrometers. In humans, ciliated surfaces are found, for example, in the respiratory tract where they sweep mucus, or in the Fallopian tubes where they move an ovum to the uterus. The motion of the fluid above a ciliated surface is generated by periodic beating of cilia. Experimental observations have shown that the beating pattern of an individual cilium is asymmetric and composed of two phases: the effective stroke, during which the outstretched cilium propels the fluid like an oar, followed by the recovery stroke, when the bent cilium returns to the initial position sweeping along the surface in a way that produces as little backward flow as possible (4). Although each cilium can beat independently, cilia densely covering a surface synchronize their cycles and form metachronal waves, thus increasing their fluid pumping efficiency (5). It is believed that the metachronal waves occur as a result of hydrodynamical interactions between the cilia (6, 7).

The efficiency of the ciliary pumping mechanism leads to the idea of using the same principle for designing artificial cilia that act as microscale pumps and mixers. An important step towards biomimetic cilia was made by Darnton et al., who created a bacterial carpet by attaching bacteria to a solid surface (8). Due to symmetric rotation and weak coordination between bacterial flagella, the flow patterns were rather complex and ever-changing. Better control over artificial cilia is obtained by driving them externally, for example, by magnetic or electric fields. The first attempt to fabricate artificial cilia was based on nanorod arrays manufactured from magnetic-polymeric composite materials (9). By using a moving permanent magnet, it was demonstrated that the nanorods can perform a simple periodic motion. Furthermore, den Toonder et al. have proven that electrostatically driven cilia made of metal-coated polymer films can act as mixers and—outside the low

Reynold's number regime—even as pumps (10, 11). Similar light-driven microactuators have recently been manufactured using azobenzene doped liquid crystals (12). As an alternative approach, soft lithography enables fabrication of regular arrays of cilia that could be actuated by an electron beam (13). Despite progress in this area, there has been no experimental demonstration of directed fluid motion induced by artificial cilia so far.

Here we report on the realization of self-assembled artificial cilia and prove that their asymmetric beating, which resembles the beating of biological cilia, generates a directed fluid flow. The artificial cilia are formed as flexible yet stable chains of superparamagnetic colloidal particles. They are held together by an external magnetic field, which not only gives structural stability to a cilium, but is also used to induce motion of cilia and thus delivers energy into the system. We show that a simple non-reciprocal beating pattern induced by conical rotation of the magnetic field results in nearly uniform fluid motion above the ciliated surface.

## Results and Discussion

**Formation of Cilia and Pumping of Fluid.** Artificial cilia were formed in a homogeneous external magnetic field as shown in Fig. 1. The external field induced magnetic dipole moments in the superparamagnetic beads that were parallel to the direction of the field. The attractive forces between the magnetic dipoles resulted in the formation of stable colloidal chains. We avoided additional bonding between individual beads [for instance by DNA fragments (14)] and retained the option of controlled disassembly of the chains in the course of the experiment.

Assembly of artificial cilia was done in two different ways: the first was to individually trap the beads by optical tweezers and arrange them into a chain (Fig. 2A), whereas the second was to let the beads self-assemble in external magnetic field (Fig. 2B). In this case, trenches in a surface coating layer were used to guide the assembly process and to control the length of the assembled chains. The trenches are clearly visible in Fig. 2B. While the practical value of the first method is limited due to the slow bead assembly and requirement of optical tweezers, the manually controlled cilia assembly is ideal for demonstration of the concept and for testing agreement with proposed theoretical models. The second method, however, has a potentially greater practical value as it enables production of large arrays of artificial cilia and only requires a varying external magnetic field. Moreover, the system is self-healing: shorter cilia can be "repaired" with the supplementing beads that are present in the surrounding fluid. Even though the self-assembled cilia do not yet reach the level of uniformity compared to the cilia assembled with optical tweezers, they show excellent pumping ability as well.

Once the colloidal chains were formed, their orientation followed the direction of the external magnetic field. By changing the magnetic field, we were able to drive the cilia in a nonreciprocal asymmetric manner, which is required for starting and sustaining fluid flow in the sample [see supporting information (SI)

Author contributions: N.O., I.P., and D.B. designed research; A.P., B.K., N.O., and A.V. performed research; M.V. and A.P. analyzed data; and M.V. and A.V. wrote the paper.

The authors declare no conflict of interest.

This article is a PNAS Direct Submission.

<sup>1</sup>To whom correspondence should be addressed. E-mail: mojca.vilfan@ijs.si.

This article contains supporting information online at [www.pnas.org/cgi/content/full/0906819106/DCSupplemental](http://www.pnas.org/cgi/content/full/0906819106/DCSupplemental).



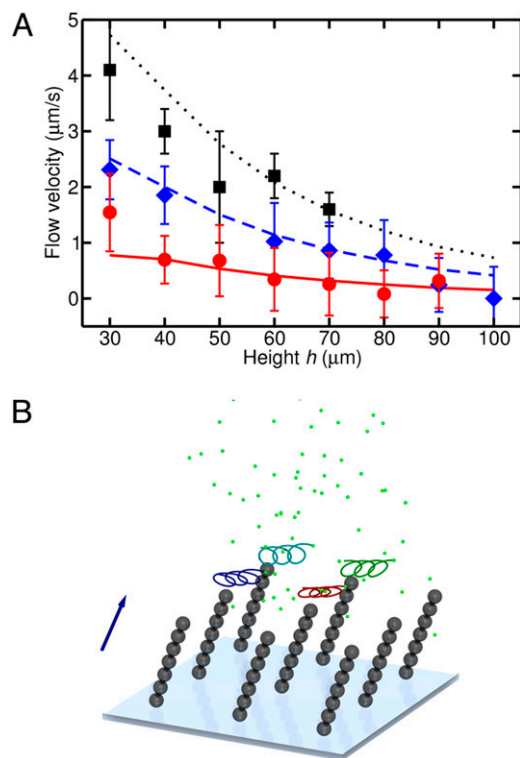


**Fig. 4.** Induced flow velocity depends on the height  $h$  above the ciliated surface. (A) Flow velocity generated by rotating cilia as a function of  $h$  for different tilt angles (rotation frequency was 0.5 Hz). Experimental data (symbols), and data obtained by a numerical simulation (lines):  $\vartheta = 20^\circ$  (● and solid line),  $\vartheta = 30^\circ$  (◆ and dashed line),  $\vartheta = 40^\circ$  (■ and dotted line). One should note that there were no free parameters in the simulation. (B) Schematic view of the numerical simulation that was done for exactly the same configuration as in the experiment and for the same parameter values. Tracer particles were randomly distributed through the sample and their average velocity was calculated. The arrow denotes the direction of the external magnetic field.

the same parameter values, e.g. the bead size and density, cilia length, separation between the cilia, bead magnetization and the external magnetic field density. Each bead was subject to gravitational, buoyant, magnetic, contact, and constraint forces. Based on the Stokes hydrodynamics, we calculated the mobility matrix for a group of particles in the presence of a solid boundary. This allowed us to determine the particle velocities at any time.

The fluid velocity was then obtained by extending the mobility matrix to include the tracer particles, which were subject to viscous forces only. A schematic view of the simulated system is shown in Fig. 4B and the animation of the system in [Movies S4–S6](#). As in the experiment, we followed the tracer particles and calculated their average velocity at a given height  $h$  above the ciliated surface in order to obtain the pumping velocity profile. While the velocity field between the cilia, i.e. for  $h < L$ , was vortical, it changed into a homogeneous flowing layer for larger elevations above the surface. The obtained data are shown in Fig. 4A as lines.

If one compares the experimentally obtained data with the results from the numerical simulation, a very good agreement is found. One should note that the simulation was not a fit to the experimental data but rather an independent calculation with no free parameters. The observed minor discrepancy likely results from inhomogeneities in the velocity profile and from the uncontrolled background flow.

In summary, we have created ordered arrays of self-assembled artificial cilia and demonstrated that they can be used to generate fluid flow in a microfluidic chamber. Both the assembly of beads into chains and their attachment to the surface are

**Table 1.** Parameters used in the numerical simulation

Parameter	Description	Value
$N$	Number of magnetic beads	63
$a$	Bead radius	2.2 μm
$\eta$	Water viscosity	0.001 Pa s
$\chi$	Magnetic susceptibility of beads	1.63
$\rho$	Mass density of beads	1,600 kg m <sup>-3</sup>
$d$	Ciliary array lattice size	28 μm
$B$	Magnetic field amplitude	1.8 mT
$\alpha$	Pumping direction	30°
$\omega/2\pi$	Rotation frequency	0.5 Hz

driven by induced magnetic forces, thus enabling disassembly—or reassembly—of the cilia during the experiment. Although the synchronized tilted conical motion of the artificial cilia in our system is very simplified in contrast to the beating pattern of real cilia, we have demonstrated that the pumping ability of such artificial ciliated surface is effective and thus suitable for microfluidic applications.

## Materials and Techniques

**Experimental Setup.** An experimental setup that allowed precise control over the magnetic field was built around an inverted optical microscope (Zeiss, Axiovert 200M, Achroplan 63/0.9W objective) equipped with optical tweezers (17, 18). For tweezing Nd:YAG laser (Coherent, Compass 2500MN) was steered by acousto-optic deflectors (A.A. Opto-electronic, DTSXY-250-1064-002) and a beam steering controller (Aresis, BSC-160). Three orthogonal pairs of water-cooled nearly Helmholtz coils were used to generate a homogeneous magnetic field within the sample. The currents through the coils were individually regulated by a six-channel current source, which enabled us to generate a homogeneous magnetic field of arbitrary direction and varying magnitude (Fig. 1 A). The typical magnetic field used in the experiments was 1.8 mT.

To ensure interaction via the external magnetic field, we used monodisperse superparamagnetic beads (Dynabeads Epoxy M-450, Dynal Biotech, diameter 4.4 μm; coated with SDS (sodium dodecyl sulfate), 5 mg/ml, 5 hrs in ultrasonic bath) (19). In order to create an array of colloidal chains that would resemble a ciliated surface, the bottom ends of the bead chains were anchored to the glass surface by an array of ferromagnetic nickel dots via magnetic attraction (Fig. 1 B). We used standard microscope glass slides that were coated with a 500-nm-thick nickel layer by sputtering and etched to create nickel anchoring sites that were 5 μm in diameter and arranged in a square lattice with 28 μm between nearest neighbors.

The tracer particles were nonmagnetic silica spheres (Bangs Laboratories, diameter 1 μm). Their movement was recorded with a CMOS camera (PixeLINK, PL-A741) and analyzed off-line using a custom-written particle tracking software to obtain their trajectories.

**Guided Self-Assembly of Artificial Cilia.** In order to guide the self-assembly process and to control the cilia length, we fabricated trenches in a 5-μm-thick layer of photoresist SU-8 2025 (Microchem, standard coating procedure, adhesion promoter TI Prime, Microchemicals GmbH). Direct illumination of the structures on the photoresist was done with a UV laser (Omikron Laserage GmbH, Bluephoton LDM375.20.CW.A.L, 375 nm). The laser beam was steered by acousto-optic deflectors (A.A. Opto-electronic, DTSXY-400-405) controlled by a beam steering controller (Aresis, BSC-160) and focused by Zeiss LD Plan-neofluar 20x/0.4 Korr objective.

Depth and width of the trenches were 5 μm, i.e. slightly larger than the diameter of the beads, so that a single chain was formed in each trench when the beads were left to sediment. The trench that was 45 μm long determined the length of an individual cilium, although some of the trenches did not fill up completely. The position of the trenches corresponded to the position of the nickel dots, so that one end of each trench had one anchoring point. Glass plates with structured photoresist were coated with BSA (bovine serum albumin, Sigma-Aldrich, 10 mg/ml in ultrapure water) to prevent adhesion of the spheres. We used 200-μm spacers to ensure uniform separation between the glass slide and a coverslip, and the cell was sealed to prevent the evaporation of the fluid.

**Numerical Simulation.** We numerically simulated the dynamics of  $N$  beads with radii  $a$ . All model parameters are listed in Table 1. We denote the position coordinates of bead  $j$  with  $\mathbf{x}_j$ . The vector  $\mathbf{r}_{jk} = \mathbf{x}_k - \mathbf{x}_j$  denotes the distance vector between beads  $j$  and  $k$ ,  $r_{jk} = |\mathbf{r}_{jk}|$  the distance between them and  $\hat{\mathbf{r}}_{jk} = \mathbf{r}_{jk}/r_{jk}$  the unit vector pointing from bead  $j$  to bead  $k$ . Each bead is subject to the gravitational, magnetic, contact and constraint force that can be expressed as

$$\mathbf{F}_j = -mg\hat{\mathbf{e}}_z + \sum_{k \neq j} \mathbf{F}_{kj}^{\text{magnetic}} + \sum_{k \neq j} \mathbf{F}_{kj}^{\text{contact}} \hat{\mathbf{r}}_{kj} + \mathbf{F}_j^{\text{constraint}}. \quad [1]$$

Here  $m$  denotes the buoyant mass of a particle

$$m = \frac{4\pi a^3}{3}(\rho - \rho_{\text{H}_2\text{O}}). \quad [2]$$

The magnetic force

$$\mathbf{F}_{kj}^{\text{magnetic}} = \frac{\mu_0}{4\pi} \left( 3 \frac{\mathbf{r}_{kj}(\mathbf{m}_k \cdot \mathbf{m}_j) + \mathbf{m}_k(\mathbf{m}_j \cdot \mathbf{r}_{kj}) + \mathbf{m}_j(\mathbf{m}_k \cdot \mathbf{r}_{kj})}{r_{kj}^5} - 15 \frac{\mathbf{r}_{kj}(\mathbf{m}_k \cdot \mathbf{r}_{kj})(\mathbf{m}_j \cdot \mathbf{r}_{kj})}{r_{kj}^7} \right) \quad [3]$$

results from the dipole–dipole interaction between induced magnetic dipoles in beads, which are proportional to the external magnetic field acting on each bead

$$\mathbf{m}_j = (4\pi a^3/3)\chi \mathbf{B}_j/\mu_0. \quad [4]$$

In this expression  $\mathbf{B}_j$  denotes the sum of the external field and the contributions of all other particles at the site of particle  $j$ :

$$\mathbf{B}_j = \mathbf{B}_{\text{ext}} + \frac{\mu_0}{4\pi} \sum_{k \neq j} \left( -\frac{\mathbf{m}_k}{r_{kj}^3} + 3 \frac{\mathbf{r}_{kj}(\mathbf{m}_k \cdot \mathbf{r}_{kj})}{r_{kj}^5} \right). \quad [5]$$

For a given configuration of particle positions  $\mathbf{x}_j$ , the magnetic moments  $\mathbf{m}_j$  can be determined in a self-consistent manner by solving the system of Eqs. 4 and 5.

The contact forces act between all pairs of beads in contact, whereas the constraint forces act on surface-anchored beads at the bottom of each chain. The contact forces can be determined in a self-consistent manner so that the radial component of the relative velocity of neighboring beads is never negative and  $\mathbf{r}_{kj} \cdot (\mathbf{v}_j - \mathbf{v}_k) = 0$  for all pairs of beads in direct contact  $(k, j)$ . Likewise, the constraint forces is determined from the requirement that the velocity of each anchored bead (the bead at the bottom of each cilium) is zero:  $\mathbf{v}_j = 0$ .

With known forces  $\mathbf{F}_j$  on all beads, the bead velocities  $\mathbf{v}_i$  follow as

$$\mathbf{v}_i = \sum_j \mu_{ij} \mathbf{F}_j, \quad [6]$$

where  $\mu$  is the mobility matrix describing the dynamics of particles in a viscous fluid in the proximity of a solid boundary. With the notation we use here it is a  $N \times N$  matrix (number of particles), whose elements are  $3 \times 3$  matrices (number of spatial dimensions). The diagonal terms  $\mu_{ii}$  describe the mobility of a single sphere in the vicinity of a wall, for which we use the following expression (20, 21)

$$\mu_{ii} = \frac{1}{6\pi\eta a} \begin{pmatrix} \beta_{ij}^{\text{tt}} & 0 & 0 \\ 0 & \beta_{ij}^{\text{tt}} & 0 \\ 0 & 0 & \alpha_{ij}^{\text{tt}} \end{pmatrix}, \quad [7]$$

with

$$\alpha_{ij}^{\text{tt}} \approx 1 - \frac{9}{8} \frac{a}{z_i} + \frac{1}{2} \left( \frac{a}{z_i} \right)^3 - \frac{1}{8} \left( \frac{a}{z_i} \right)^5 \quad [8]$$

and

$$\beta_{ij}^{\text{tt}} \approx 1 - \frac{9}{16} \frac{a}{z_i} + \frac{1}{8} \left( \frac{a}{z_i} \right)^3 - \frac{1}{16} \left( \frac{a}{z_i} \right)^5, \quad [9]$$

where  $\eta$  is the fluid viscosity and  $z_i$  the height of the particle  $i$  above the surface.

Off-diagonal terms describe the velocity of particle  $i$ , induced by a force acting on particle  $j$ . If the two particles are small in comparison with the distance between them, they are given by the Blake tensor (22)

$$\mu_{ij}^{\text{Blake}} = \frac{1}{8\pi\eta} \left( \mathbf{G}^S(\mathbf{x}_i - \mathbf{x}_j) - \mathbf{G}^S(\mathbf{x}_i - \bar{\mathbf{x}}_j) + 2z_j^2 \mathbf{G}^D(\mathbf{x}_i - \bar{\mathbf{x}}_j) - 2z_j \mathbf{G}^{SD}(\mathbf{x}_i - \bar{\mathbf{x}}_j) \right) \quad [10]$$

with

$$\mathbf{G}_{\alpha\beta}^S(\mathbf{r}) = \frac{\delta_{\alpha\beta}}{r} + \frac{\mathbf{r}_\alpha \mathbf{r}_\beta}{r^3}, \quad [11]$$

$$\mathbf{G}_{\alpha\beta}^D(\mathbf{r}) = (1 - 2\delta_{\beta z}) \frac{\partial}{\partial r_\beta} \left( \frac{\mathbf{r}_\alpha}{r^3} \right), \quad [12]$$

$$\mathbf{G}_{\alpha\beta}^{SD}(\mathbf{r}) = (1 - 2\delta_{\beta z}) \frac{\partial}{\partial r_\beta} \mathbf{G}_{\alpha z}^S(\mathbf{r}). \quad [13]$$

Here  $\bar{\mathbf{x}}_j$  denotes the mirror image of the position of particle  $j$ : if  $\mathbf{x}_j$  has the coordinates  $\mathbf{x}_j = (x, y, z)^T$ , it is defined as  $\bar{\mathbf{x}}_j = (x, y, -z)^T$ . For finite-sized particles, a better result is obtained using the Rotne–Prager approximation (23). In the presence of a wall, we follow the approach from ref. 21 and calculate the off-diagonal mobility matrix elements as

$$\mu_{ij} = \left( 1 + \frac{a^2}{6} \nabla_{\mathbf{x}_i}^2 \right) \left( 1 + \frac{a^2}{6} \nabla_{\mathbf{x}_j}^2 \right) \mu_{ij}^{\text{Blake}}. \quad [14]$$

We give the explicit form of these expressions in [SI Text: Mobility Matrix](#).

As in the experiment, the magnetic field followed the time dependence described with the following expression

$$\mathbf{B}_{\text{ext}}(t) = \begin{pmatrix} \cos \alpha & -\sin \alpha & 0 \\ \sin \alpha & \cos \alpha & 0 \\ 0 & 0 & 1 \end{pmatrix} \times \begin{pmatrix} \cos \vartheta & 0 & \sin \vartheta \\ 0 & 1 & 0 \\ -\sin \vartheta & 0 & \cos \vartheta \end{pmatrix} \times \begin{pmatrix} -\sin \psi \cos(\omega t) \\ \sin \psi \sin(\omega t) \\ \cos \psi \end{pmatrix}. \quad [15]$$

The resulting system of differential equations was solved numerically using the Euler method.

**ACKNOWLEDGMENTS.** We thank J. Kotar for his contribution to the magnetic tweezers and P. Panjan for Ni-coated plates. This work was supported by the Slovenian Research Agency Grants P1-0192, P1-0099, J1-0908 and J1-2200, and in part by the European Social Fund of the European Union. M.V. was supported by NATO Reintegration Grant EAP.RIG.981424.

- Squires TM, Quake SR (2005) Microfluidics: Fluid physics at the nanoliter scale. *Rev Mod Phys* 77:977–1026.
- Whitesides GM (2006) The origins and the future of microfluidics. *Nature* 442:368–373.
- Purcell EM (1977) Life at low Reynolds number. *Am J Phys* 45:3–11.
- Gray J (1928) *Ciliary Movement* (Cambridge Univ Press, Cambridge, UK).
- Gueron S, Levit-Gurevich K (1999) Energetic considerations of ciliary beating and the advantage of metachronal coordination. *Proc Natl Acad Sci USA* 96:12240–12245.
- Gueron S, Levit-Gurevich K, Liron N, Blum JJ (1997) Cilia internal mechanism and metachronal coordination as the result of hydrodynamical coupling. *Proc Natl Acad Sci USA* 94:6001–6006.
- Vilfan A, Jülicher F (2006) Hydrodynamic flow patterns and synchronization of beating cilia. *Phys Rev Lett* 96:058102.
- Darnton N, Turner L, Breuer K, Berg HC (2004) Moving fluid with bacterial carpets. *Biophys J* 86:1863–1870.
- Evans BA, et al. (2007) Magnetically actuated nanorod arrays as biomimetic cilia. *Nano Lett* 7:1428–1434.
- Khatavkar VV, Anderson PD, den Toonder JMJ, Meijer HEH (2007) Active micromixer based on artificial cilia. *Phys Fluids* 19:083605–13.
- den Toonder J, et al. (2008) Artificial cilia for active micro-fluidic mixing. *Lab Chip* 8:533–541.
- van Oosten CL, Bastiaansen CWM, Broer DJ (2009) Printed artificial cilia from liquid-crystal network actuators modularly driven by light. *Nat Mater* 8:677–682.
- Pokroy B, Epstein AK, Persson-Gulda MCM, Aizenberg J (2009) Fabrication of bioinspired actuated nanostructures with arbitrary geometry and stiffness. *Adv Mat* 21:463–469.
- Dreyfus R, et al. (2005) Microscopic artificial swimmers. *Nature* 437:862–865.
- Downton MT, Stark H (2009) Beating kinematics of magnetically actuated cilia. *Europhys Lett* 85:44002.
- Smith DJ, Blake JR, Gaffney EA (2008) Fluid mechanics of nodal flow due to embryonic primary cilia. *J R Soc Interface* 5:567–573.
- Kotar J, et al. (2006) Interparticle potential and drag coefficient in nematic colloids. *Phys Rev Lett* 96:207801.
- Vilfan M, et al. (2008) Confinement effect on interparticle potential in nematic colloids. *Phys Rev Lett* 101:237801.
- Fonnum G, Johansson C, Molteberg A, Morup S, Aksnes E (2005) Characterisation of Dynabeads by magnetization measurements and Mossbauer spectroscopy. *J Magn Magn Mater* 293:41–47.
- Perkins GS, Jones RB (1992) Hydrodynamic interaction of a spherical particle with a planar boundary: II. Hard wall. *Physica A* 189:447–477.
- Gauger EM, Downton MT, Stark H (2009) Fluid transport at low Reynolds number with magnetically actuated artificial cilia. *Eur Phys J E Soft Matter* 28:231–242.
- Blake JR (1971) A note on the image system for a stokeslet in a no-slip boundary. *Proc Camb Phil Soc* 70:303–310.
- Rotne J, Prager S (1969) Variational treatment of hydrodynamic interaction in polymers. *J Chem Phys* 50:4831–4837.